Revista do Programa de Pós-Graduação em Geografia da Universidade Federal do Piauí

MAPPING OF ABOVE-GROUND BIOMASS BY REMOTE SENSING AND MACHINE LEARNING IN MANGROVES OF THE PARNAÍBA RIVER DELTA, NORTHEASTERN BRAZIL

Jéssica Cristina Oliveira **FROTA**
Doutoranda em Desenvolvimento e Meio Ambiente (PRODEMA/UFPI)
E-Mail:Jessicauapi@Gmail.Com
Orcid: https://orcid.org/0000-0001-5314-8058

Gustavo Souza **VALLADARES**
Professor Doutor Associado da UFPI. Departamento de Geografia
E-mail:valladares@ufpi.edu.br/
Orcid: https://orcid.org/0000-0002-4884-6588

Rabech Grasiely Gomes **MARQUES**
Professora na Secretaria Municipal de Teresina (SEMEC) E-mail:
rabechgrasiely1998@hotmail.com;
Orcid: https://orcid.org/0000-0003-3597-8634

Léya Jéssika Rodrigues Silva **CABRAL**
Doutoranda em Desenvolvimento e Meio Ambiente- E-mail:
leyarodriguescabral@gmail.com;
Orcid: http://orcid.org/0000-0001-7141-9210

Mirya Grazielle Torres **PORTELA**
Professora EBTT Universidade Federal do Piauí (UFPI), Floriano, Brasil
E-mail: mirya.portela@ufpi.edu.br/
Orcid: https://orcid.org/0000-0001-5605-7151

Recebido
Novembro de 2024

Aceito
Junho de 2025

Publicado
Dezembro de 2025

Abstract: Mangrove ecosystems represent important carbon sinks, known as blue carbon. They promote climate balance by regulating greenhouse gas concentrations. Methods that use allometric equations, remote sensing and machine learning have been increasingly employed to quantify biomass. Thus, the objective of this study was to estimate the spatial distribution of above-ground plant biomass (AGB) present in mangroves of the Parnaíba River Delta, located in northeastern Brazil. For this, 27 plots were sampled, each measuring 200 m². In each plot, data of diameter at breast height and height of each individual, and AGB was estimated using allometric equations. The spatial distribution of AGB was mapped by means of modeling, and it was possible to extract and select spectral variables obtained from images from the Landsat 8-9 and Sentinel-2 satellites. For the predictive analysis, the algorithms were used: Multiple Linear Regression, XGBoost, Random Forest, Cubist, Earth and Support vector machine (linear, radial and polynomial). It was observed that the mangrove vegetation of the species Rhizophora mangle obtained the highest AGB, with 790 Mg ha-¹, and the model that best fitted the prediction to was XGB, but the best fit was obtained for the dry period, with R^2= 0.93, RMSE = 66.74 Mg ha-1 and MAE of 49.42 Mg ha-1. The MSI sensor also showed a very strong fit for the XGB model, with R^2 = 0.92 Mg ha-1, RMSE = 64.02 Mg ha-1 and MAE of 46.31 Mg ha-1, indicating lower errors, probably due to its higher spatial resolution.

Keywords: allometry; *blue carbon*; carbon stock; ecological stress; modeling.

MAPEAMENTO DA BIOMASSA ACIMA DO SOLO POR SENSORIAMENTO REMOTO E APRENDIZADO DE MÁQUINA EM MANGUEZAIS DO DELTA DO RIO PARNAÍBA, NORDESTE DO BRASIL

Resumo: Os ecossistemas de mangue representam importantes sumidouros de carbono, conhecidos como carbono azul. Promovem o equilíbrio climático regulando as concentrações de gases com efeito de estufa. Métodos que utilizam equações alométricas, sensoriamento remoto e aprendizado de máquina têm sido cada vez mais empregados para quantificar a biomassa. Assim, o objetivo deste estudo foi estimar a distribuição espacial da biomassa vegetal acima do solo (BGA) presente em manguezais do Delta do Rio Parnaíba, localizado no Nordeste do Brasil. Para isso foram amostradas 27 parcelas, cada uma medindo 200 m². Em cada parcela foram estimados os dados de diâmetro à altura do peito e altura de cada indivíduo, e AGB por meio de equações alométricas. A distribuição espacial do AGB foi mapeada por meio de modelagem, sendo possível extrair e selecionar variáveis espectrais obtidas a partir de imagens dos satélites Landsat 8-9 e Sentinel-2. Para a análise preditiva foram utilizados os algoritmos: Regressão Linear Múltipla, XGBoost, Random Forest, Cubista, Terra e Máquina de vetores de suporte (linear, radial e polinomial). Observou-se que a vegetação de manguezal da espécie Rhizophora mangle obteve o maior AGB, com 790 Mg ha-¹, e o modelo que melhor se ajustou à previsão foi o XGB, mas o melhor ajuste foi obtido para o período seco, com R^2= 0,93, RMSE = 66,74 Mg ha-1 e MAE de 49,42 Mg ha-1. O sensor MSI também apresentou ajuste muito forte para o modelo XGB, com R^2 = 0,92 Mg ha-1, RMSE = 64,02 Mg ha-1 e MAE de 46,31 Mg ha-1, indicando menores erros, provavelmente devido à sua maior resolução espacial.

Palavras-chave: alometria; carbono azul; estoque de carbono; estresse ecológico; modelagem.

MAPEO DE LA BIOMASA AÉREA MEDIANTE TELEDETECCIÓN Y APRENDIZAJE AUTOMÁTICO EN MANGLARES DEL DELTA DEL RÍO PARNAÍBA, NORESTE DE BRASIL

Resumen: Los ecosistemas de manglares representan importantes sumideros de carbono, conocidos como carbono azul. Promueven el equilibrio climático regulando las concentraciones de gases de efecto invernadero. Para cuantificar la biomasa se han utilizado cada vez más métodos que utilizan ecuaciones alométricas, teledetección y aprendizaje automático. Así, el objetivo de este estudio fue cuantificar y estimar la distribución espacial de la biomasa vegetal aérea (BGM) presente en los manglares del delta del río Parnaíba, ubicado en el noreste de Brasil. Para ello se muestrearon 27 parcelas de 200 m² cada una. En cada parcela se estimaron datos de diámetro a la altura del pecho y altura de cada individuo, y AGB mediante ecuaciones alométricas. Se mapeó la distribución espacial del AGB mediante modelación y fue posible extraer y seleccionar variables espectrales obtenidas de imágenes de los satélites Landsat 8-9 y Sentinel-2. Para el análisis predictivo se utilizaron los siguientes algoritmos: Regresión Lineal Múltiple, XGBoost, Random Forest, Cubista, Tierra y Máquina de Vectores de Soporte (lineal, radial y polinómico). Se observó que la vegetación de manglar de la especie Rhizophora mangle obtuvo el mayor AGB, con 790 Mg ha-¹, y el modelo que mejor ajustó la predicción fue el XGB, pero el mejor ajuste se obtuvo para el período seco, con R^2 = 0.93, RMSE = 66.74 Mg ha-1 y MAE de 49.42 Mg ha-1. El sensor MSI también mostró un ajuste muy fuerte para el modelo XGB, con R^2 = 0,92 Mg ha-1, RMSE = 64,02 Mg ha-1 y MAE de 46,31 Mg ha-1, lo que indica errores menores, probablemente debido a su mayor ajuste espacia resolución.

Palabras clave: alometría; carbono azul; stock de carbono; estrés ecológico; modelación.

INTRODUCTION

Coastal environments are areas of relevant environmental fragility, where the elements that make up the functioning and stability of the systems respond to a complex dynamic, resulting from the interaction of continental and coastal agents. These environments are home to a set of ecosystems of high environmental relevance that end up performing extremely important functions, whether of ecological, social or economic nature. The mangrove, for example, is a coastal ecosystem that is located in a zone of transition between the terrestrial and marine environments and that provides favorable conditions for the development of many animal species, besides being considered an important transformer of nutrients in organic matter (Pinto *et al.*, 2017).

Mangroves also represent important carbon sinks, known as blue carbon (Kuwae *et al.* 2022; Tang *et al.*, 2016). In other words, this vegetation plays an important role in sequestering carbon from the atmosphere and can regulate greenhouse gas concentrations.

With the increase in carbon levels in the atmosphere, it has become necessary to understand the capacity of mangroves to store carbon, in order to bring alternatives to the climate imbalance caused in the environment (Adame *et al.*, 2015; Donato *et al.*, 2011). Although studies on this topic are still limited, especially with regard to the behavior of carbon in mangrove vegetation in the most diverse biomes, some studies seek to understand the occurrence of this dynamic. To this end, strategies have been developed to overcome these obstacles, applying methodologies with the use of allometric equations, empirical studies, and simple and complex models associated with sensing through machine learning (ML).

The establishment of allometry is of fundamental importance, as it contributes to the floristic knowledge and evaluation of the plant species present, thus providing elements for developing the ordering of quantitative aspects of the vegetation that is still little known, especially the mangrove vegetation (Arruda; Daniel, 2007).

In addition, geotechnologies and the use of modeling, which are important tools to facilitate environmental analysis, have been bringing relevance in the analysis and mapping of mangrove areas, enabling the generation of products with good cartographic accuracy and precision. Different parametric and non-parametric statistical models have been used to predict mangrove biomass. However, as pointed out by Tian *et al*. (2022), the prediction precision of non-parametric approaches is often better because they do not make assumptions about the distribution of the data, as is the case with many ML methods.

The ML algorithm is characterized by making predictions on data through training and making independent decisions based on the construction of a model based on a set of selected predictors. Models such as XGB, RF and CB are based on a decision tree and are widely used in AGB estimation.

MLR is a statistical technique that simultaneously analyzes more than one variable related to an object of study. The ET model, according to Kuhn and Johnson (2013), seeks to model the nonlinear relationships between predictors and continuous responses that do not require specifications of the exact form of nonlinearity before its application to training data, while the SVM model tries to find hyperplanes that separate the data and, according to dos Santos (2018), this algorithm differs from others by not directly estimating probabilities but the class of the response of interest for a new observation.

These models use terrestrial data and allometric equations to develop biomass estimates to train those models that best fit, based on remote sensing data (Jachowski *et al*., 2013; Wu et al., 2016; Pham *et al*., 2018; Meier *et al*., 2018; Li *et al.*, 2017; Li *et al*., 2020; Ghosh; Behera, 2021; Siqueira *et al.*, 2021).

Given the above, the study raises the hypothesis that the application of machine learning algorithms to remote sensing data significantly improves the accuracy of mangrove vegetation biomass estimates compared to traditional field data collection methods. Thus, knowing that biomass estimation studies help in better understanding and finding solutions to climate issues, the present study aims to estimate the spatial distribution of AGB present in the mangroves of the Parnaíba River Delta Environmental Protection Area, located on the coast of northeastern Brazil, through the use of machine learning.

MATERIAL AND METHODS

Characterization of the study area

The area under study corresponds to the mangroves present in the Parnaíba River Delta Environmental Protection Area (PRD EPA), which is located in the lower Parnaíba sub-basin. The PRD EPA comprises the extreme west coast of Ceará, portions along the entire length of the coast of Piauí and the extreme east coast of Maranhão. It occupies an approximate area of 313,809 hectares, with a perimeter of 472.80 km, entirely covering the municipalities of Cajueiro da Praia (PI) and Ilha Grande (PI) and partially covering the municipalities of Parnaíba (PI), Luís Correia (PI), Barroquinha (CE), Chaval (CE), Água Doce do Maranhão (MA), Araioses (MA), Paulino Neves (MA) and Tutóia (MA) (Figura 1).

Figure 1 – Map of location map of mangroves in the Parnaíba River Delta Environmental Protection Area

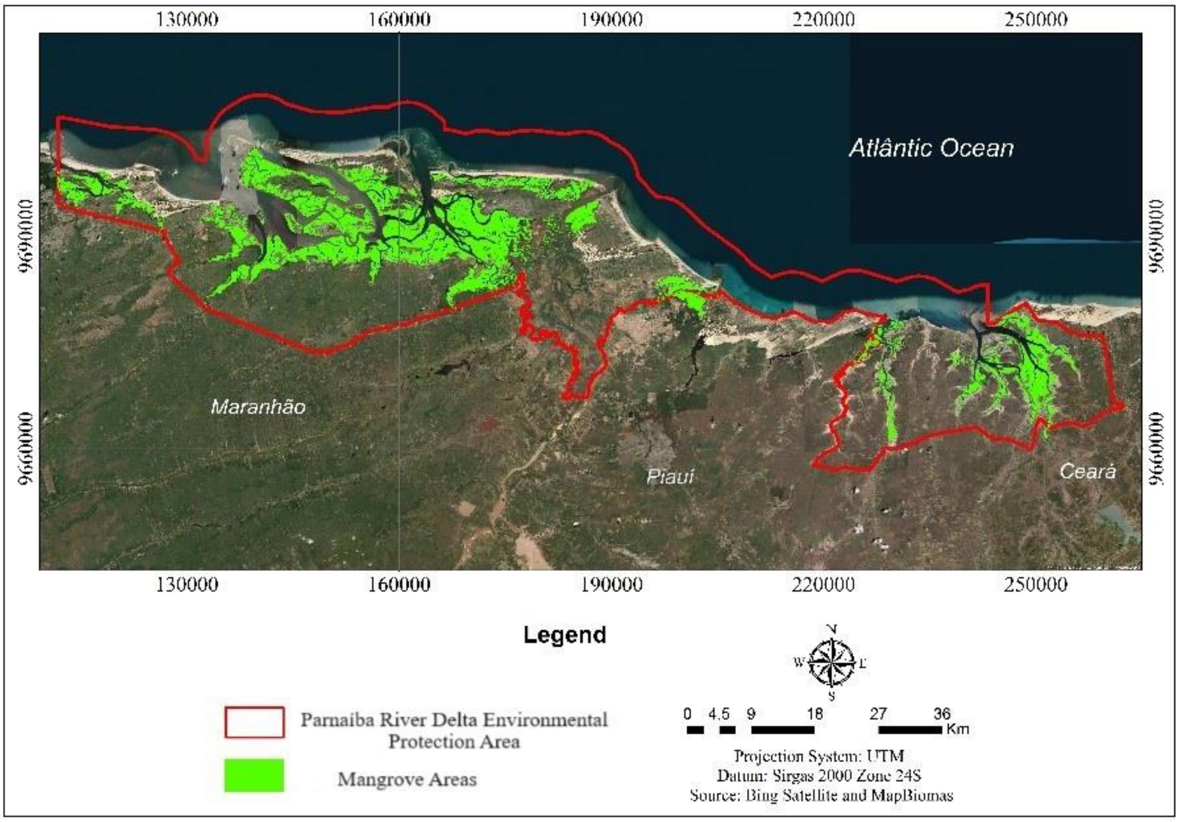

Fonte: Os autores (2024).

In addition to the conservation unit (CU) of the PRD EPA, in the study area there is also an overlap of three other CUs: EPA of Foz do Rio Preguiças – Pequenos Lençóis, a CU of the Maranhão state (State Decree 11.899 of June 11, 1991); Parnaíba River Delta Marine Extractive Reserve (RESEX) (Federal Decree of November 16, 2000); and the Ilha do Caju Private Natural

Heritage Reserve (RPPN) (Ordinance 96-N-DOU 214-E -0 9/11/1999 - section/pg. 1/26) (ICMBIO, 2020).

The PRD EPA was created through the Federal Decree of August 28, 1996 and is under the responsibility of the Chico Mendes Institute for Biodiversity Conservation (ICMBIO). According to Guzzi (2012), this area is characterized by having a mosaic of ecosystems intersected by bays and estuaries, in addition to being a dynamic fluvial-marine region, formed by the ecological tension between Cerrado, Caatinga and marine systems. In addition, it has a strong Amazonian influence in its portion of Maranhão (west) and the semi-arid region in Ceará (east). Almost 25% of its territory is made up of jurisdictional waters and with a population of approximately 360,000 inhabitants (ICMBIO, 2020).

Considering the hydrological, geological, pedological and geomorphological factors, there are four landscape units within the EPA area: dune field, fluvial-marine plain, river plain and coastal tablelands. The areas of the fluvial-marine plain are responsible for transporting matter and energy carried by the rivers, tides, and rainfall that are so important for that system (da Silva, 2020)

Although the area under study is located in representative areas of Cerrado and Caatinga vegetation, it has a continuous system of mangroves, which help in the control of coastal erosion and in the stabilization of fine sediments, hence reducing the capacity and competence of rivers in the transport of sediments. The main mangrove species observed in the EPA area are: red mangrove (*Rhizophora mangle*), white mangrove (*Laguncularia racemosa*), button mangrove (*Conocarpus erectus*), 'siriba' or 'sereiba', black mangrove or 'siriba' mangrove and white 'siriba' (*Avicennia germinans* and *Avicennia schaueriana*) (Guzzi, 2012; Andrade *et al.*, 2014; Flora do Brasil, 2020; Nascimento, 2021).

Abreu *et al.* (2019) point out that the EPA area has a varied rainfall regime with isohyets between 1000 and 1600 mm per year, which goes from January to May. From August to November, lower rainfall indices are recorded, demonstrating that the monthly rainfall regime has a unimodal distribution with minimum rainfall in August and maximum in April, and the main atmospheric system acting in the region is the Intertropical Convergence Zone (ITCZ). The main economic activity carried out in the study area is subsistence fishing, which involves the collection of fish, crabs, shrimps, oysters and shellfish, family farming, animal husbandry and the extractivism of seeds and fruits. It is worth mentioning that the EPA is also part of the Route of Emotions tourist itinerary, which also covers the Jericoacoara National Park, in Ceará, and the Lençóis Maranhenses National Park, in Maranhão.

Choice of sampling points to define the plots

The sampling points were defined based on a random stratified strategy, considering the areas with greater representativeness in relation to vegetation structure. Maps were produced using images from the orbital sensors of the Landsat-8 OLI (Operational Land Imager) and RapidEye images as a way to better visualize the geographical area that corresponds to the EPA area. To choose the points, the of mangrove vegetation was also spatialized by interpreting the normalized difference vegetation index (NDVI), using the same strategy adopted by Portela *et al.* (2020), sampling plots with variability for NDVI. Thus, 27 plots were installed (Figura 2), each measuring 200 m² (10x20), and all of which are representative of the mangrove vegetation.

Figure 2 - Map of distribution of plots in mangrove areas of the Parnaíba River Delta Environmental Protection Area

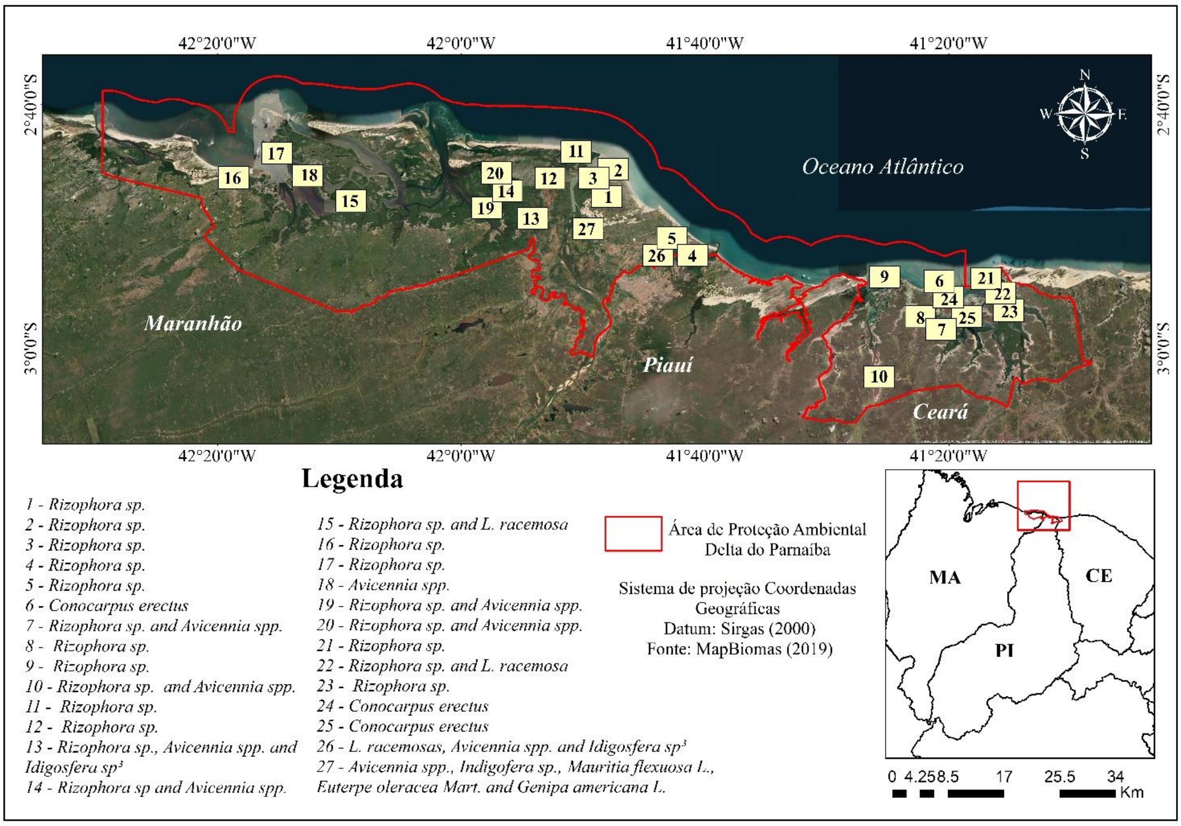

Fonte: Os autores (2024).

Procedures for field determination of AGB data

To determine the above-ground plant biomass (AGB), a survey on the characteristics of the vegetation was carried out through a population census, collecting information regarding the height of trees and diameter at breast height (DBH) of each individual. The AGB of the mangrove area of the EPA was calculated based on allometric equations for living vegetation (Table 1), according to the species identified and adopted in other similar studies (Kauffman & Donato, 2012; Portela *et al.*, 2020; Nascimento, 2021).

Table 1 - Allometric equations used to determine living plant biomass in different mangrove species

SPECIES	EQUATIONS	REFERENCES
Laguncularia recemosa	Biom (kg)= 0,1023 X DBH $^{2.5}$	(Fromard *et al.*, 1998)
Avicennia sp.	Biom (kg)= 0,14 x DBH $^{2.4}$	(Fromard *et al.*, 1998)
Conocarpus erectus	Biom (kg)= 0,1023 X DBH $^{2.5}$	(Fromard *et al.*, 1998)
Rizophora sp.	In (Biom. (kg)) = 14,867663 = 0,5132 In (área basal ^{2} x H)	(Santos *et al.*, 2017)
Other species (DBH 3≥30 cm)	Biom (kg) = 0,1730 x DBH,^{2,2950}	(Lima Júnior et al. 2014)

To analysis the AGB of dead species standing or fallen within the plots, the equation proposed by Fundación Solar (2000) was used in an adapted form. The litter biomass was determined by the direct method (Fundación Solar, 2000), where, in each plot, a 0.3 m² circumference was randomly thrown three times, collecting all the material contained within it.

AGB estimation by remote sensing and machine learning

The analysis of spatial distribution of AGB by remote sensing was carried out using the method proposed by Lu *et al.* (2005) and Lima Júnior (2014) with adaptations, with extraction and selection of spectral variables from images from the Landsat 8-9 OLI sensor, orbit/point 218/62 and the Sentinel-2 satellite. These data were correlated with the field biomass estimates, because according to Naessens *et al.* (2012), in the process of calibration and validation of the data, the model used is confronted with the field data and the prediction can be confirmed.

In the case of the Landsat 8-9 images, they were downloaded from the USGS (United States Geological Survey) website and correspond to the dry season on 09/15/2018 and the rainy season on 03/22/2023. It is important to highlight that both data were collected at Level-2, taking into account the occurrence of atmospheric correction. Acquisition and pre-processing of the Sentinel-2/MSI images were carried out on the GEE (Google Earth Engine) platform, where the chosen historical series dates from August 1 to November 30, 2021, also with atmospheric correction. Processing of the images and obtaining of the final products from the methodological procedures were carried out using the following software programs: ESRI ArcGIS® 10.3, QGIS and R Studio version 4.3.2 (R Core Team, 2020).

After acquisition of the images, the bands B1, B2, B3, B4, B5, B6 and B7 (OLI) were grouped in a single file called "*Stack*" in the statistical program R to perform a composition of bands. The same procedure was performed for bands B2, B3, B4, B5, B6, B7, B8A, B11 and B12 of Sentinel-2. From the bands, the following spectral indices were calculated based on the literature by George *et al.* (2018), Tran, Ruth and Zuh (2022), Santos (2018) and Ramírez (2015) serving as input data to estimate biomass: RVI, NDVI, EVI, NDWI, SAVI, GNDVI, MNDWI, CTVI, CLAY and IRON (Table 2).

Table 2 - Representation of the equations used to determine spectral indices

ÍNDICE	EQUATION	REFERENCES
Ratio Vigor Index (RVI)	$RVI = \frac{NIR}{RED}$	Pearson e Miller (1972)
Normalized Difference Vegetation Index (NDVI)	NDVI = $\frac{NIR-RED}{NIR+RED}$	Rouse *et al.*, (1973)
Soil-adjusted Vegetation Index (SAVI)	SAVI= $\frac{NIR-RED}{NIR+RED+L}$ *(1 + L)	Huete (1988)
Enhanced Vegetation Index (EVI)	EVI = G$\left(\frac{NIR-RED}{NIR+C1*RED-C2*BLUE+L}\right)$	Huete et al., (1997)
Normalized difference water index (NDWI)	NDWI = $\frac{GREEN-NIR}{GREEN+NIR}$	Gao (1996)
Green Normalized Difference VegetationIndex (GNDVI)	GNDVI = $\frac{NIR-GREEN}{NIR+GREEN}$	Gitelson *et al.*, (1996)
Modified Normalized Difference Water Index (MNDWI)	MNDWI = $\frac{GREEN-Swir2}{GREEN+ Swir2}$	Xu (2006)
Corrected Transformed Vegetation Index (CTVI)	CTVI = $\frac{(NDVI+0,5)}{\lvert NDVI+5 \rvert} * \sqrt{\lvert NDVI+5 \rvert}$	Perry e Lautenschlager (1984)
Clay Minerals (CLAY)	CLAY = $\frac{BANDA\ 6}{BANDA\ 7}$	Sabins (1997)
Iron Oxide (IRON)	IRON = $\frac{RED}{BLUE}$	Sabins (1997)

Nota: NIR: Banda infravermelha próxima; RED: Faixa vermelha; GREEN: Faixa verde; BLUE: Faixa azul; Swir2: Faixa infravermelha de onda curta (1400-1800nm); G: Fator de ganho = 2,5; L: Fator de correção para solo, onde foi utilizado o valor = 0,25 no índice SAVI e o valor = 1 no índice EVI; C1 e C2: Coeficientes de ajuste para efeito de aerossol atmosférico, onde C1 = 6 e C2 = 7,5; As bandas 6 e 7 no cálculo de Clay podem variar dependendo do satélite (Landsat 8-9 ou Sentinel-2). Fonte: Adaptado de Portela, 2019; Amorim, 2019.

To calculate these indices, it was necessary to install the *raster* package through the *install.packages* ("*raster*") tool and use R software. For the predictive analysis, the following machine learning algorithms were used: Multiple Linear Regression (MLR), Random Forest (RF), XGBoost (XGB), Cubist (CB), Earth (ET) and Support vector machine (SVM – linear, radial and polynomial), adapted from the literature, in order to test and investigate which model had the best prediction performance.

In addition, it is worth mentioning that the models were tested using all variables (bands and indices) and all algorithms were implemented through the Caret package. Prediction error was calculated by the *leave-one-out cross-validation* (LOOCV) methodology, as employed by Jachoswi *et al.* (2013) and Selvaraj and Pérez (2023).

The performance of the estimates, i.e., how the algorithm is performing, was evaluated using validation measures recommended by Whang *et al.* (2016) such as the coefficient of determination (R^2), root mean squared error (RMSE) and mean absolute error (MAE). In addition to these statistical metrics, the evaluation of the models was performed through the visual analysis of the scatter plots between the observed AGB values and the values predicted by the models. After that, AGB was mapped for the entire study area, for models with better performance and using R software.

RESULTS AND DISCUSSION

Estimation of mangrove biomass using field data and allometry

For the estimation of AGB in the field, through the survey of the species carried out in the 27 plots, it was possible to observe the presence of 626 individuals, distributed in four genera and five species of mangrove*: Rhizophora spp.*, *Laguncularia racemose*, *Conocarpus erectus*, *Avicennia germinans* and *Avicennia schaueriana.* It is worth pointing out that these last two species were not differentiated through taxonomic study and, for the estimation of AGB, they were considered only as *Avicennia* spp. The same occurs with the genus *Rhizophora* spp.

In some plots, 23 individuals of species such as: Indigofera sp; Mauritia flexuosa L., Euterpe oleracea Mart. and Genipa americana L. Totaling 649 individuals. It is also important to highlight that the survey covers an area of 5,400 m² of a total of approximately 413 km^2 of mangrove areas included in the PRD APA (MapBiomas Project, 2021). Through the (Figura 3) it is possible to observe the biomass value found in each of the sampled plots.

Figure 3 shows a minimum of 8 Mg ha^{-1}, a maximum of 789 Mg ha^{-1} and a mean of 258 Mg ha^{-1}. Similar data were also found by Jachowski *et al.* (2013), who estimated the plant biomass of mangroves in southwestern Thailand and found an average value of 250 Mg ha^{-1}. These data are higher than those reported by Wong *et al.* (2020), who found average AGB of about 197 Mg ha^{-1} in northern Malaysia.

Figure 3 - Distribution of above-ground biomass stock observed in the field in different plots. Plot of Rizophora sp. - 1, 2, 3, 4, 5, 8, 9, 11, 12, 16, 17, 21, 23; Plots of Rizophora sp. and *Avicennia spp.* – 7, 10, 13, 14, 19, 20; Plots of Rizophora sp. *and L. racemosa* - 15, 22; *C. erectus* plots - 6, 24, 25; Avicennia spp. - 18; Plot of *L. racemosa and Avicennia spp.* – 26.

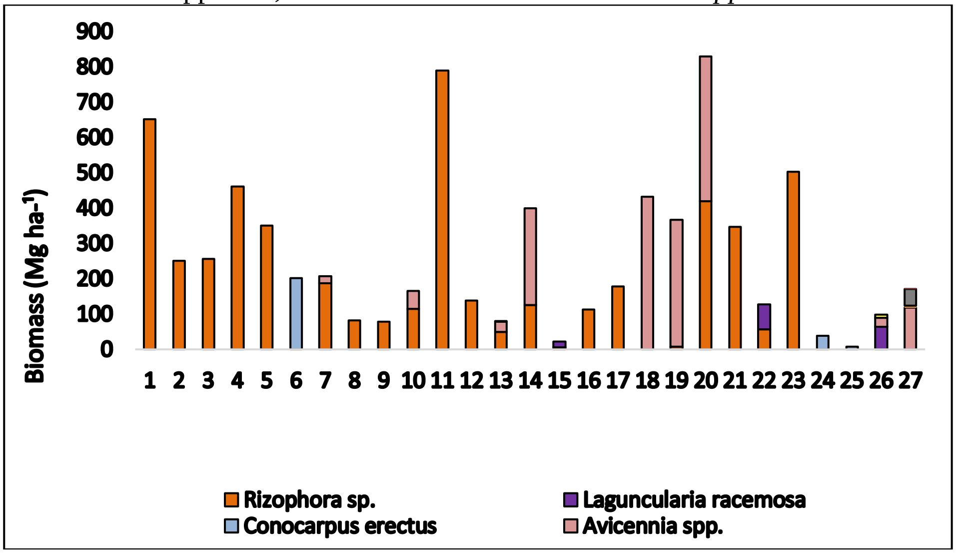

Fonte: Os autores (2024).

(2018) in their studies concluded that a semi-arid community in northwestern Australia contained an average of 70 Mg ha^{-1} of AGB. Tian *et al.* (2022), when evaluating the AGB of mangroves in a subtropical estuary of the Maoling River, Guangxi, China, observed that the AGB of the invasive mangroves showed a high spatial distribution pattern in the northwest and low spatial distribution pattern in the southeast, and its value ranged from 7 Mg ha^{-1} to 114 Mg ha^{-1}, with an average of 26 Mg ha^{-1}. Fujimoto *et al.* (2022), in a study conducted in the mangrove forests of Micronesia, observed that, in the *Rhizophora stylosa* community characterized by stilt roots, the highest AGB was estimated at 895 Mg ha^{-1}, a value considered the highest of all existing data from terrestrial survey in the tropics. Through this study it can be observed that tropical areas also present relevant values and averages of AGB in mangroves.

In Brazil, estimates of blue carbon stocks do not include the entire area of mangroves present, but studies such as the one conducted by Bernadino *et al.* (2024) reveal an estimate of AGB in a portion of the mangrove vegetation in the Amazon ranging from 29 to 335 Mg C ha^{-1}. Kalffman *et al.* (2018), in turn, found a mean AGB value of 290 Mg ha^{-1} for the Amazon region. Santos and Beltrão (2019) estimated and compared AGB on Ajuruteua Island, Bragança, PA, in 2008 and 2018, and found values of approximately 451 Mg ha^{-1} for 2008 and 290 Mg ha^{-1} for 2018, which points to a reduction of approximately 35.7% in biomass between 2008 and 2018.

Portela *et al.* (2020) point out that the evergreen mangrove vegetation in the Parnaíba River Delta had the highest mean value for plant biomass, 517.43 Mg ha^{-1}. Braga *et al.* (2024), when estimating AGB in the mangrove forest of the Pacoti River, in the State of Ceará, found that 16.60 tons were stored in the 1,119 plants analyzed. The species with the highest amount of biomass was *Rhizophora mangle*, which accounted for about 71% of the total mass found.

The plot under study with the highest value of AGB (plot 11) has 12 predominant individuals of the same genus (*Rizophora sp.*), mean diameter of 35 cm and mean height of 13.33 m, indicating greater biomass in species that have larger diameters, as observed in the boxplot (Figura 4) through the maximum, minimum, mean and standard deviation values presented. This result was also observed by Pinto *et al.* (2017), who analyzed the sequestration of atmospheric carbon in the mangrove forest of the EPA of Serra do Guararú, in São Paulo, and pointed out that the carbon stored in the form of biomass is directly proportional to DBH.

Similar data were also presented by Fontoura *et al.* (2017), who observed biomass variations between the compartments of the mangrove vegetation, according to the increase in DBH. In the study area, the number of individuals and height were also important attributes in the composition of AGB.

Figure 4 - Boxplot of different values of maximum, minimum, mean and standard deviation in the mangrove plots of Parnaíba River Delta Environmental Protection Area. (a) DHP values, (b) height values, (c) biomass values

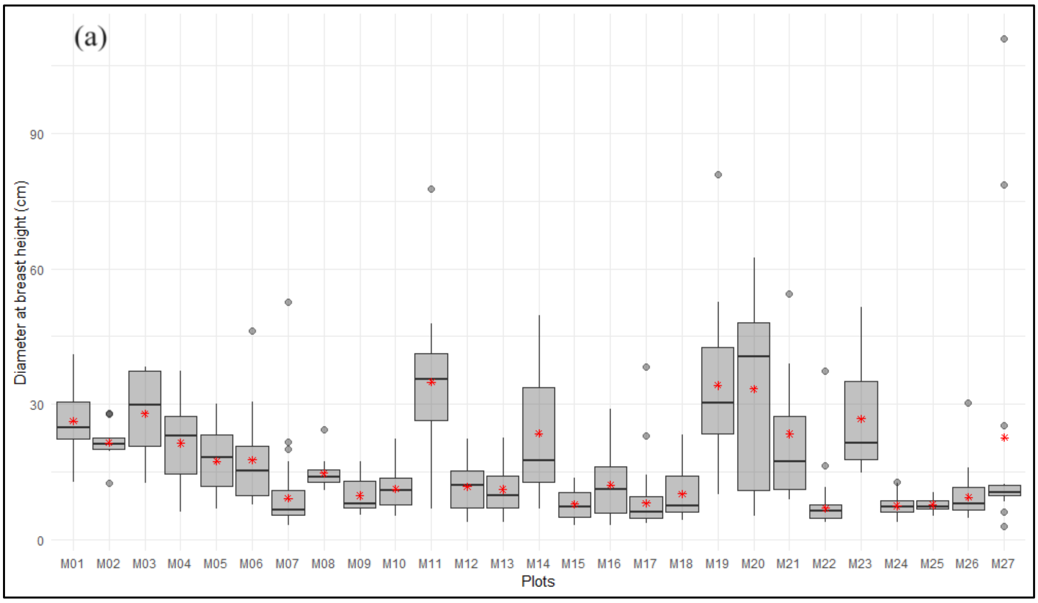

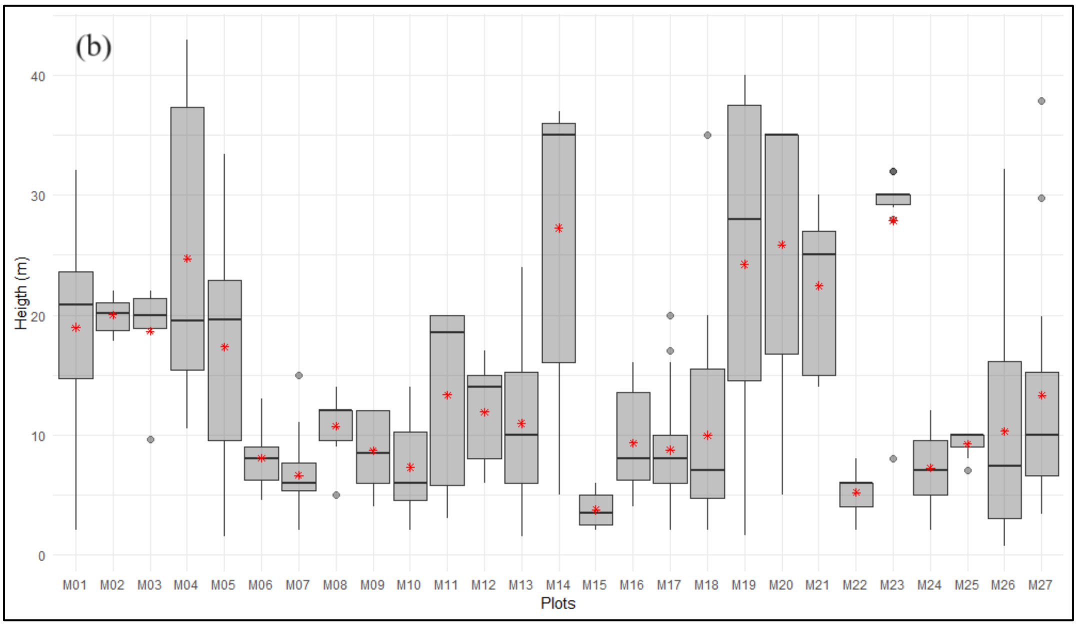

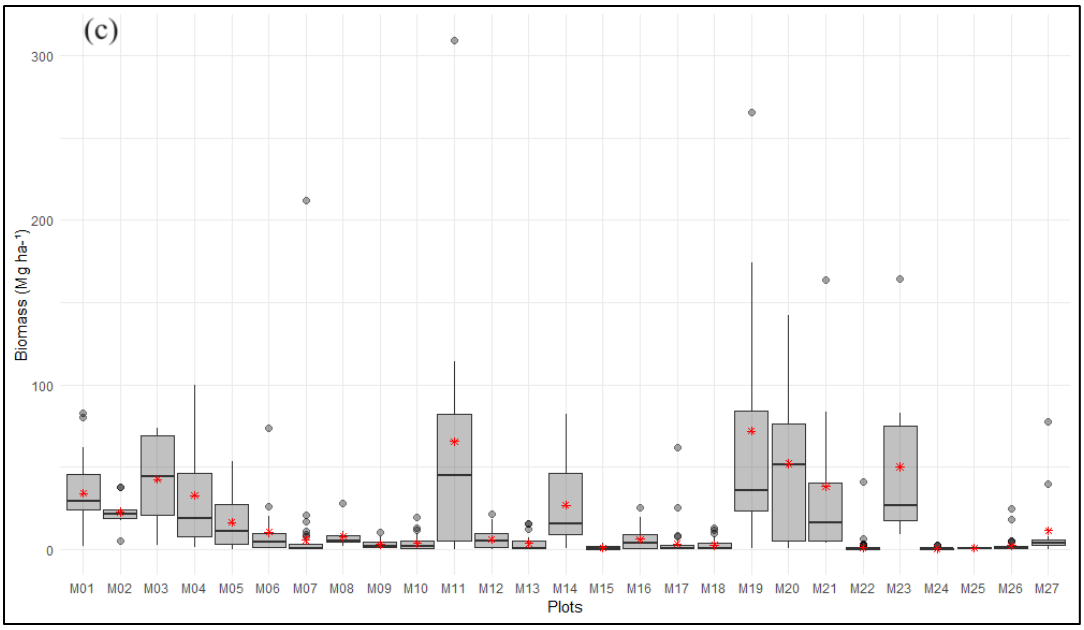

Fonte: Os autores (2024).

By observing these data, it was possible to confirm that the highest biomass estimates are associated with *Rizophora sp.* and *Avicennia* spp., since both reached values above 700 Mg ha^{-1}. These species, represented in plots 11 and 19, also had in some individuals DBH of 77.67 cm for *Rizophora sp.* (plot 11) and maximum height of the individuals of 20 m and DBH of 80.85 cm for *Avicennia* spp. (plot 19), with mean of 34.14 cm, maximum height of 40 m reached in their individuals and mean of 24.23 m (Figura 5).

Figure 5 - A: Representation of the species *Rizophora sp.*; B: Representation of *Avicennia spp*

Fonte: Os autores (2024).

Plots 25, 15 and 24 were the ones with the lowest biomass values compared to the others, respectively 8 Mg ha^{-1}, 23 Mg ha^{-1} and 38 Mg ha^{-1}. These plots, in turn, have a mean DBH ranging from 7.41 cm to 8 cm and mean height ranging from 4 m to 9.22 m. Two of these plots (24 and 25) together with plot 6 are representative of *C. erectus* and have mostly crooked and thin trunks and branches (Figura 6).

Figura 6 - Diameter measuring the height of the breast of the representative portion of *Conocarpus erectus*; B: fruit of the species *Conocarpus erectus*

Fonte: Os autores (2024).

C. erectus has greenish flowers and gray or brown bark. They occupy elevated portions of the terrain and are rarely hit by the tides. They are also considered species that have the highest resistance among mangrove woods and were widely used for the manufacture of shipbuilding parts and firewood production (ICMBIO, 2018).

It is worth mentioning that, in the study area, these species were only found in mangroves that comprise the East side of the PRD EPA area, with plots 6 and 24 installed in the municipality of Cajueiro da Praia, PI, and plot 25 in the municipality of Barroquinha, CE. In mangrove forests in southeastern Mexico, AGB was higher in this species (*C. erectus*) (253.18±32.17 Mg·ha^{-1}) and lower in other species, such as *A. germinans* (161.93±12.63 Mg ha^{-1}). This occurred because the species *C. erectus* grew on more elevated terrains in the region, where soils were richer in nutrients (Santos *et al.* 2014).

Avicennia spp. only occurred predominantly in plot 18 and had AGB value of 79 Mg ha^{-1}, while *L. racemosa* vegetation was mixed with other species, in three plots (15, 22 and 26), thus contributing to the biomass estimate.

Based on the survey carried out and the species found, it can be highlighted that the species R. mangle is responsible for 75% of the AGB produced, followed by *Avicennia spp*. with approximately 19%, *C. erectus* with 4% and *L. racemosa* with 2%. In addition, the variation of biomass in the analyzed plots is directly linked to the changes in the variables involved in the allometric equations presented in this study. Therefore, it can be seen that the oscillation of biomass throughout the area is also linked to the different species of mangrove and their characteristics.

Estimation of mangrove biomass using Landsat 8-9/OLI and Sentinel-2/MSI remote sensing images and machine learning.

For biomass estimation using Landsat 8-9 and Sentinel-2 remote sensing images, the biomass obtained in the field was considered a dependent variable and the reflectance values (bands) and spectral indices derived from the images were considered independent variables. Once all the covariates were selected, it was possible to evaluate the most important ones presented by the ML models in R software. When the most important variables for the model resulted in better validation, these models were presented (Table 3).

Table 3 – Erros estatísticos de predição calculados para cada modelo representando a AGB de bosques de mangue da APA do Delta de Parnaíba, PI com imagens do Landsat 8-9 e Sentinel-2

Machine Learning Model	Variables explanatory	RMSE (Mg/ha)	MAE (Mg/ha)	R²	Máx.	Mín.
Landsat -8/ OLI						
Random Forest	B2 + NDWI+ B1 + B3 + IRON+B4	107.24	87.36	0.86	522.43	73.33
Random Forest	All	110.37	88.25	0.86	520.10	80.51
XGBoost	**All**	**66.74**	**49.42**	**0.93**	**677.29**	**20.04**
Regressão Linear Multipla	All	134.31	89.92	0.61	676.97	-2.16
Cubist	All	207.3	147.3	0.16	287.44	75.29
Regresão Earth	All	196.46	157.06	0.17	312.64	-27.2
SVM Linear	All	195.77	129.29	0.20	441.53	-13.83
SVM Radial	All	169.98	96.94	0.48	453.63	30.07
SVM Polinomial	All	206.65	144.43	0.18	266.39	30.12
Landsat - 9/ OLI						
Random Forest	B2+B3+B4+B5+IRON +CLAY	107.86	84.7	0.87	-	-
Random Forest	All	115.47	93.57	0.85	502.55	82.14
XGBoost	**All**	**84.20**	**60.24**	**0.88**	**639.16**	**2.21**
Regressão Linear Multipla	All	134.78	97.42	0.61	652.42	-50.41
Cubist	All	200.86	148.98	0.17	310.35	105.63
Regresão Earth	All	197.56	159.44	0.16	306.56	-1.29
SVM Linear	All	197.46	130.66	0.22	368.41	-65.06
SVM Radial	All	152.21	87.92	0.56	-	-
SVM Polinomial	All	201.51	132.33	0,20	-	-
Sentinel -2 /MSI						
Random Forest	B5 +B11+ IRON+ EVI+B12+ B8A	100.09	71.87	0.86	552.63	56.2
Random Forest	All	99,32	69.51	0.88	539.07	61.29
XGBoost	All	71.89	51.58	0.92	695.23	32.65
XGBoost	**B5 + B4 + B6 + B11 + B3 + IRON**	**64.02**	**46.31**	**0.92**	**716.53**	**41.17**

Fonte: Os autores (2024).

Knowing that ML algorithms are used with the objective of estimating and minimizing the reducible error, it can be observed in Table 2 that the best model trained for AGB estimation, using all covariates, was that obtained with XGB during the dry season with Landsat-8 images, showing very good values of validation and maximum and minimum. XGB was also the best model when using Landsat-9 data from the rainy season, with very good performance.

In relation to the MSI sensor, the XGB model also showed a very strong performance, using all the variables and also taking into account the important variables. In the selection, lower MAE and RMSE values were obtained when compared to the OLI sensor, which can be explained by the higher spatial resolution compared to the Landsat 8-9 images (10 m and 30 m); however, all predictions produced strong fits, emphasizing the quality of ML modeling (Figura 7 and Table 3).

Figure 7 - Validação cruzada dos valores de AGB usando diferentes dados de sensores remoto

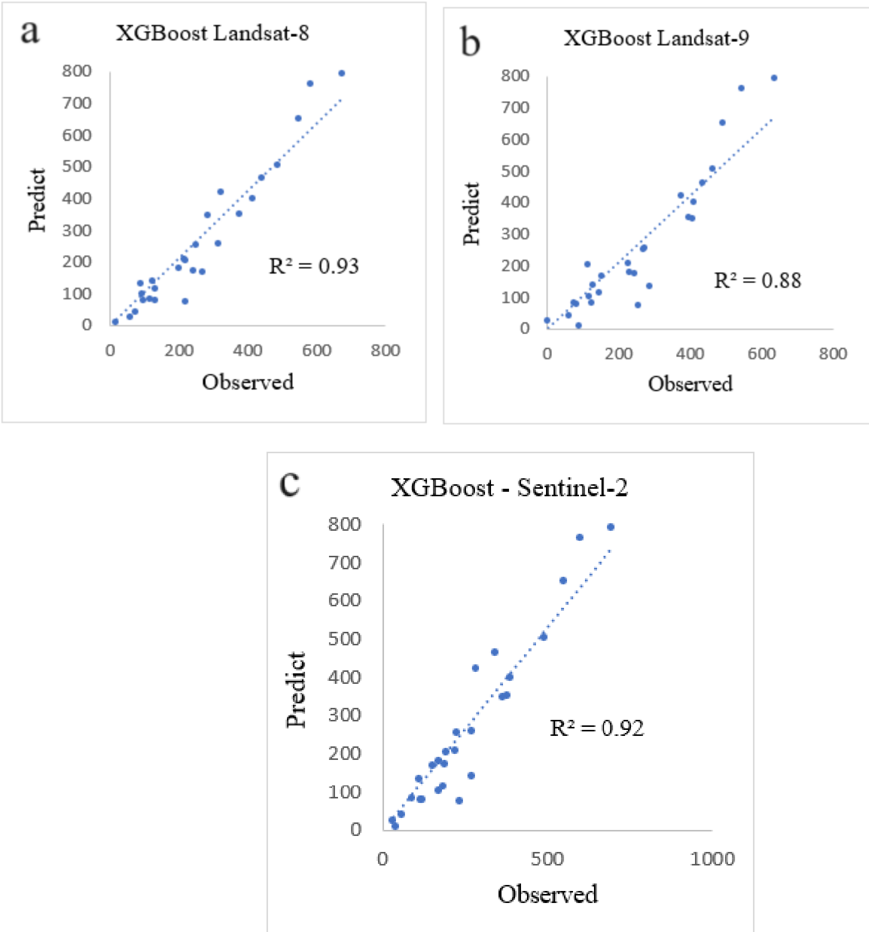

Fonte: Os autores (2024).

The distribution of most of the points around the trend line confirms the ability of the XGB model to predict with a high degree of accuracy the AGB of the mangroves in the study area. However, our results showed only a slight difference in prediction performance between the XGB and RF models. RF had excellent performance and fit in the class of very strong fit, which can also be confirmed by the studies conducted by Askne *et al.* (2017) in northern Sweden, Tian *et al.* (2021) in the Beibu Gulf, David *et al.* (2022) in Chobe National Park, Botswana, and Fararoda *et al.* (2021) in forests of India.

Li *et al.* (2020), when estimating the biomass of subtropical forests in Hunan Province, China, observed that after performing parameter fitting, there was a significant effect on the performance of the XGB algorithm compared to RF and after fitting, the R^2 of the XGB model achieved the best results ($R^2 = 0.75$).

Tian *et al.* (2021) used eight ML models to estimate the AGB of different mangrove species in the Beibu Gulf and also compare their accuracy. The best fit model found by the authors, as well as in the study carried out, was also the XGB, with R^2 = 0.83 and RMSE = 22.76 Mg ha^{-1}, followed by the RF model (R^2 = 0.78, RMSE = 25.51 Mg ha^{-1}).

Luo *et al.* (2021), when comparing the performance of different combinations of resource selection methods and algorithms, observed that the XGB model also showed an excellent performance in the estimation of AGB, with RMSE of 28.81 Mg ha^{-1}.

It is also worth mentioning that the other models presented in Table 1 were tested, but were not successful, showing low coefficient of determination with the remote sensing data variables for the Landsat 8-9 images and increasingly high errors, providing no explanations for the research data, except for the MLR model, which had R^2 = 0.61 in the Landsat 8-9 images with a moderate fit. Thus, due to the poor performance of the other models, only the XGB and RF models were fitted for the Sentinel-2 images.

The results also reveal that, among the fitted models, the correlation between AGB and the oxide index indicated that more hydromorphic soils, with few oxides, result in higher values of AGB. For Sentinel-2, band 5 (*Vegetation Red Edge 1*) played a major role in the estimation of AGB, which was also identified by (Astola *et al.*, 2019).

Da Silva *et al.* (2021), when analyzing the potential of Sentinel-2 images in estimating the biomass of *Tectona grandis L.f.* in the Western Amazon, found that Sentinel-2 images are accurate and useful for monitoring forest biomass. Pandit *et al.* (2018), when estimating AGB in protected forest areas in Nepal, pointed out that in these areas the problem of multispectral data saturation due to the large amount of biomass is common, but the Sentinel-2 data were able to overcome this problem due to the high spatial resolution and *red-edge* bands of the MSI sensor, which reinforces its capacity and effectiveness in biomass estimates.

Dang *et al.* (2019), when estimating AGB in Yok Don National Park, Vietnam, using ML, observed that in validation, the RF model developed with 11 variables was able to predict AGB with R^2 = 0.81, RMSE = 36.67 Mg ha^{-1} and RMSE = 19.55% using both Landsat and Sentinel-2 images.

The results found in the present study demonstrated exactly the same; the two sensors acted with great potential, and in the dry season this estimate is more representative, with this model, since, according to (Fitz, 2008), the decrease in the amount of water causes degradation of the photosynthetic pigments, making the leaf less likely to absorb electromagnetic radiation, which in turn will result in increased reflectance values by the sensors. Thus, as the moisture of the leaf decreases, the reflectance power in the infrared increases, proving the results found.

The map (Figura 8) shows the final result of the estimation of AGB of the PRD EPA mangrove through the Landsat 8-9 and Sentinel-2 satellites. On the maps, it is possible to observe variability of biomass and spatial distribution.

Thus, it can be observed that for the two sensors and seasons (dry and rainy) there is a large spatial correlation that coincides, where areas that correspond to the northwest of the municipality of Araioses, MA, northwest region of the municipality of Ilha Grande, PI, areas close to the Parnaíba River and a good part of the mangroves located in Barroquinha, CE, are the ones with the highest estimates of AGB, since the indices and bands show a higher spectral reflectance in the near-infrared region, resulting in a greater interaction of the incident energy.

Figure 8 - AGB estimation map in APA DPHB mangrove areas using different sensors and machine learning. (a): XGBoost model using Landsat-8 imagery, (b): XGBoost model using Landsat-9 imagery, (c): XGBoost model using Sentinel-2 images

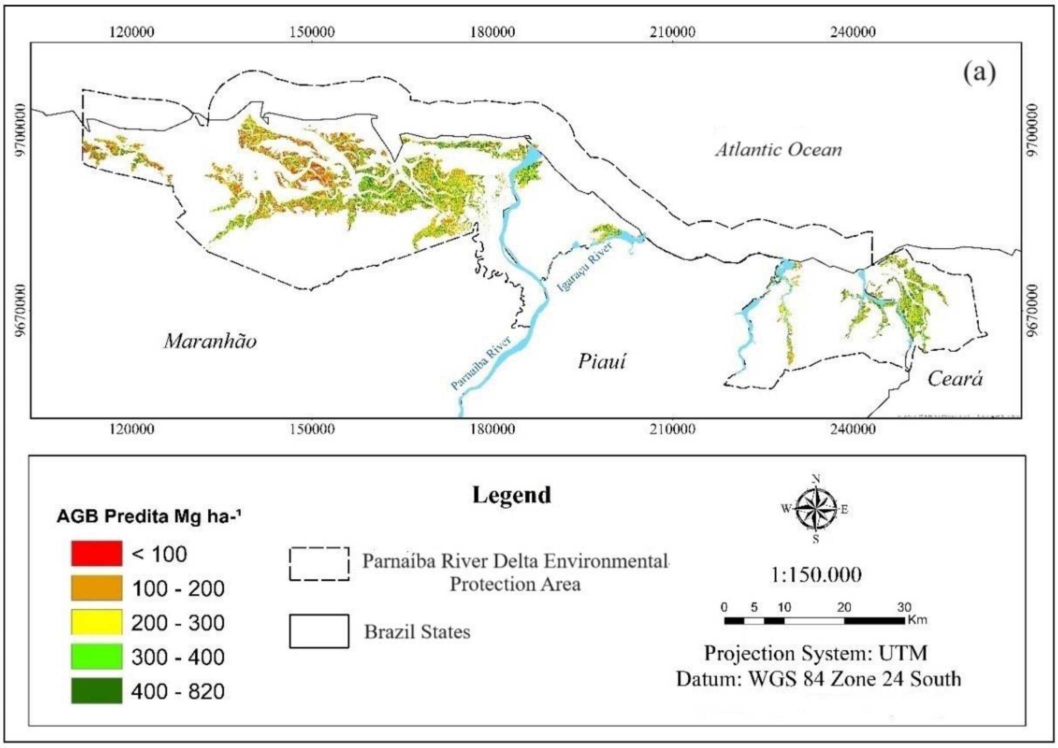

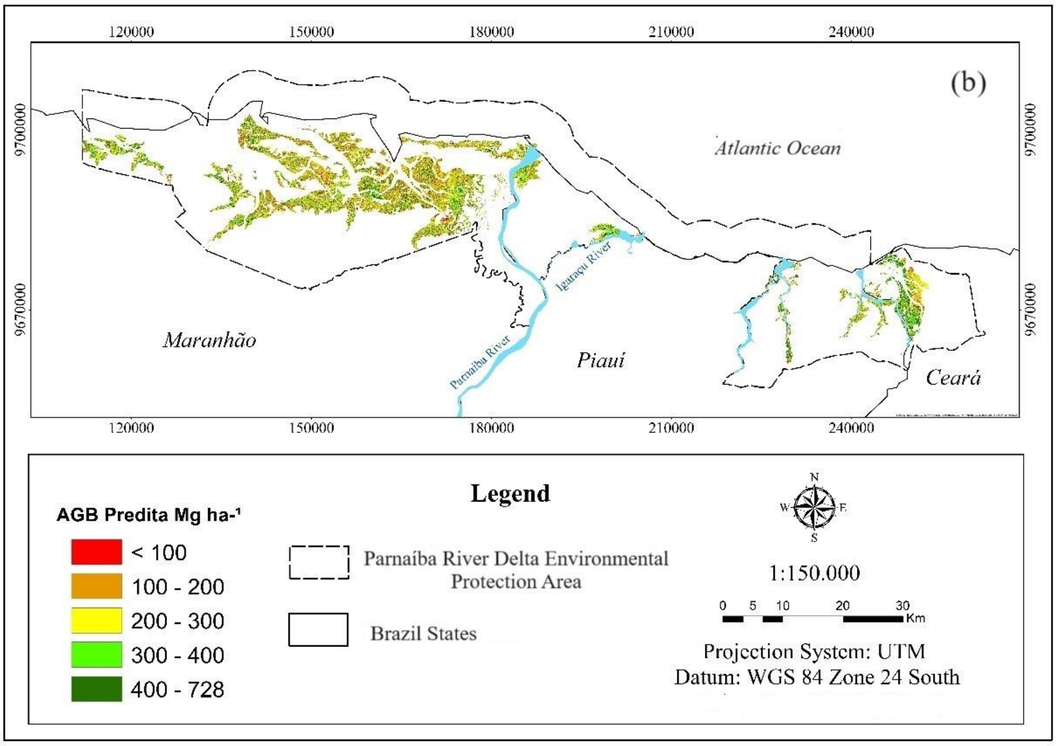

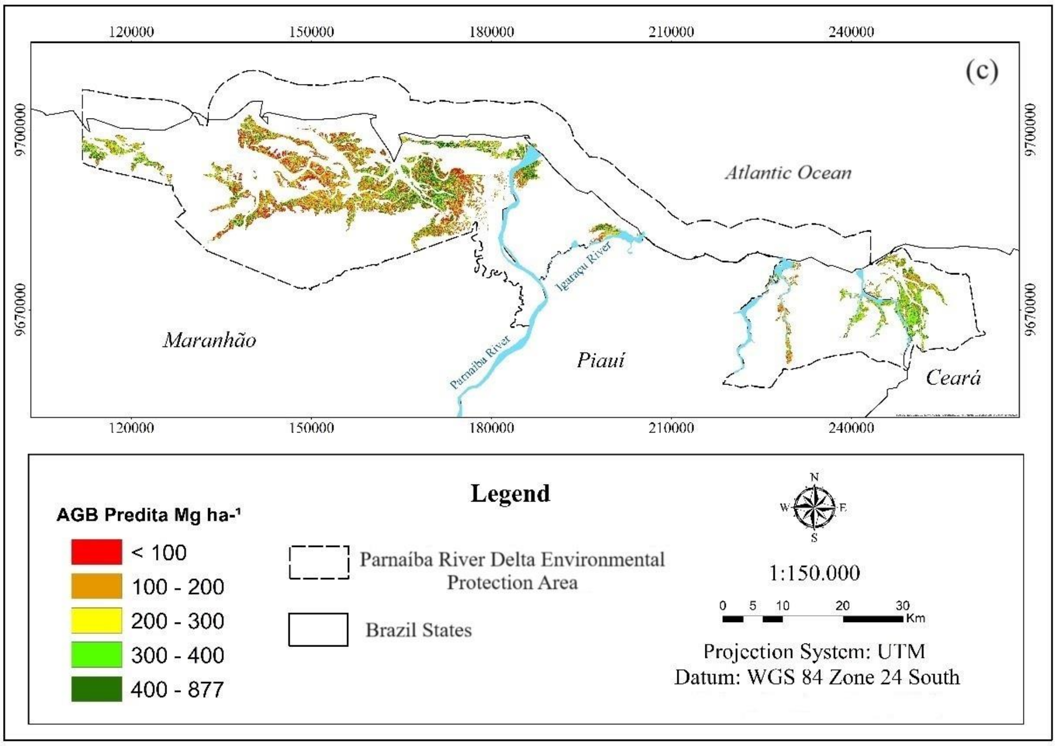

Fonte: Os autores (2024).

In addition, most of them are areas close to the mouth of rivers, where there is a large input of sediments and consequent production of nutrients that can contribute to a higher production of AGB. It can be observed that the model brought an estimate very close to the observed value, predicting biomass values of approximately 800 Mg ha^{-1}.

CONCLUSION

The estimation and spatialization of AGB in the mangroves of the study area, through remote sensing and machine learning, was efficient and indicated low uncertainty in the estimates.

The fitted models indicated good performances of OLI and MSI sensors in AGB estimation. The XGB model fitted better to the data from the two sensors, but obtained better accuracy during the dry season, with $R^2 = 0.93$, RMSE = 66.74 Mg ha^{-1} and MAE = 49.42 Mg ha^{-1}. It is worth pointing out that the Landsat-9 and Sentinel-2 images also produced excellent results, indicating a strong fit according to the literature, which highlights the quality that can be obtained from freely available images. Due to the higher spatial resolution of Sentinel-2, this sensor can be considered as the most suitable and reliable in AGB mapping.

The RF model also showed very strong fit results, especially when using Sentinel-2 images, representing the best fit of this model, with $R^2 = 0.88$ when using all variables, which can probably be explained by its better spatial resolution compared to the Landsat images.
These results suggest that the XGB and RF regression models generated have a satisfactory capacity to predict the AGB of the Parnaíba River Delta EPA, providing the basis for the planning of the relevant forestry decision-making departments.

REFERÊNCIAS

ABREU, J. M. S.; CRAIG, J. M.; ALBERT, J. S; PIOESKI, N. M. *Historical biogeography of fishes from coastal basins of Maranhão State, northeastern Brazil*. ***Neotropical Ichthyology***, [*S. l.*], v. 1, n. 2, p. 1-10, 2019. DOI: https://doi.org/10.1590/1982-0224-20180156. Acesso em: 18 fev. 2023.

ADAME, M. F; SANTINI, N. S; TOVILLA, C.; VÁSQUEZ-LULE; CASTRO, L.; GUEVARA, M. *Carbon stocks and soil sequestration rates of tropical riverine wetlands.* ***Biogeosciences,*** [*S. l.*], v. 12, n. 12, p. 3805-3818, 2015. DOI: https://doi.org/10.5194/bg-12-3805-2015. Acesso em: 18 fev. 2023.

ANDRADE A. J.P. de; SILVA, N. M. da; SOUZA, C. R. de. As percepções sobre as variações e mudanças climáticas e as estratégias de adaptação dos agricultores familiares do Seridó potiguar. **Desenvolvimento e Meio ambiente,** [*S. l.*], v. 31, n. 3, p. 77-96, ago. 2014. DOI: 10.5380%2Fdma.v31i0.32955. Acesso em: 18 fev. 2023.

ARRUDA L., OMAR, D. Florística e diversidade em um fragmento de floresta estacional semidecidual aluvial em Dourados, MS. **Floresta**, Curitiba, v. 37, n. 2, p. 189-199, mai./ago. 2007. DOI: https://doi.org/10.5380/rf.v37i2.8649. Acesso em: 18 fev. 2023.

ASKANE JAN, I. H.; SOJA, M. J.; ULANDER, L. M. H. *Biomass estimation in a boreal forest from Tan DEM-X data, lidar DTM, and the interferometric water cloud model*. ***Remote Sensing Environment,*** [*S. l.*], v. 196, p. 265-278, Jul. 2017**.** DOI: https://doi.org/10.1016/j.rse.2017.05.010. Acesso em: 18 fev. 2023.

ASTOLA, H.; HAME, T.; SIRRO, L.; MOLINIER, M.; KILPI, J. *Comparison of Sentinel-2 and Landsat 8 imagery for forest variable prediction in boreal region*, ***Remote Sensing of Environment***, [*S. l.*], v. 223, p. 257-273. DOI: https://doi.org/10.1016/j.rse.2019.01.019. Acesso em: 18 fev. 2023.

BERNARDINO, A. F; MAZZUCO, A. C. A; COSTA, R. F.; SOUZA, F.; OWUOR, M. A.; NOBREGA, G. N.; SANDERS, C. J; FERREIRA, T. O.; KAUFFMAN, J. B. *The inclusion of Amazon mangroves in Brazil's REDD+ program*. ***Nature Communications***, [*S. l.*], v. 15, n. 1549, p. 2024). DOI: https://doi.org/10.1038/s41467-024-45459-w. Acesso em: 18 fev. 2023.

BRAGA, M. M.; OLIVEIRA, J.; MORO, M. F.; BRANCO, M. S. D. Manguezais como estoques de carbono: biomassa acima do solo e o potencial econômico desse estoque na floresta de mangue do rio Pacoti, Ceará. **Caderno de Geografia**, [*S. l.*], v. 34, n. 77. DOI: https://doi.org10.5752/p.2318-2962.2024v34n77p450. Acesso em: 18 fev. 2023.

BRASIL. **Decreto nº 11.900 de 11 de junho de 1991**. Cria a Area de proteção ambiental da Foz do Rio Preguiça, abrangendo parte dos municípios de Barreirinhas, Paulino Neves, Água Doce do Maranhão, Tutóia e Araioses, Diário Oficial da União, Brasília, DF, 1991. Disponível em: https://documentacao.socioambiental.org/ato_normativo/UC/303_20100823_145738.pdf. Acesso em: 18 fev. 2023.

BRASIL. **Decreto de 28 de Agosto de 1996**. Dispõe sobre a criação da Área de Proteção Ambiental Delta do Parnaíba, nos Estados do Piauí, Maranhão e Ceará e da outras providências, Diário Oficial da União, Brasília, DF, 1996.

BRASIL. **Portaria nº 96 de 9 de novembro de 1999**. Reconhece, mediante registro, como Reserva Particular do Patrimônio Natural a Reserva denominada Ilha do Caju, situado no Município de Araioses Estado do Maranhão, Diário Oficial da União, Brasília, DF, 1999. Disponível em: https://sistemas.icmbio.gov.br/simrppn/publico/detalhe/290/. Acesso em 18 de fev. de 2023.

BRASIL. **Decreto de 16 de novembro de 2000**. Cria a Reserva Extrativista Marinha do Delta do Parnaíba, no Município de Ilha Grande de Santa Isabel, Estado do Piauí e nos Municípios de Araióses e Água Doce, Estado do Maranhão, e da outras providências, Diário Oficial da União, Brasília, DF, 2000. Disponível em:https://www.planalto.gov.br/ccivil_03/DNN/DNN9084. Acesso em 28 de março de 2023.

DANG, A.T. N.; NANDY, S.; SRINET, R.; LOUNG, N.V.; GHOSH, S.; KUMAR, A. S. *Forest aboveground biomass estimation using machine learning regression algorithm in Yok Don National Park, Vietnam*. ***Ecological Informatics***. [*S. l.*], v. 50, p. 24-32, 2019. https://doi.org/10.1016/j.ecoinf.2018.12.010. Acesso em 18 de fev. de 2023.

DAVID, R.M., ROSSER, N. J.; DONOGHUE, D. N. M. *Improving above Ground Biomass Estimates of Southern Africa Dryland Forests by Combining Sentinel-1 SAR and Sentinel-2 Multispectral Imagery*. ***Remote sensing of environment.*** [*S. l.*], v. 282, 2022. Disponível em: https://doi.org/10.1016/j.rse.2022.113232. Acesso em 18 de fev. de 2023.

DONATO, D. C.; KAUFFMAN, J. B.; MURDIYARSO, D.; KURNIANTO; S.; STIDHAM, M.; KANNINEN, M. *Mangroves among the most carbon-rich forests in the tropics.* ***Nature Geoscience.*** [*S. l.*], v. 4, p. 293-297, 2011. Disponivel em: https://doi.org/10.1038/ngeo1123. Acesso em 18 de fev. de 2023.

FARARODA, R.; REDDY, R. S.; RAJASHEKAR, G.; KIRAN CHAND, T. R., JHA, C. S.; DADHWAL, V. K. *Improving forest above ground biomass estimates over Indian forests using multi source data sets with machine learning algorithm.* ***Ecological Informatics***, [*S. l.*], v. 65, 2021. Disponível em: https://doi.org/10.1016/j.ecoinf.2021.101392. Acesso em: 7 nov. 2024.

FITZ, P. R. **Geoprocessamento sem complicação**. São Paulo: Oficina de Textos, 2008

FONTOURA, M. R.; CARON, B. O.; ELOY, E.; TREVISAN, R.; TRAUTENMÜLLER, J. W.; BEHLING, A. Modelos alométricos para estimativa de biomassa em área de regeneração natural de Ateleia Glazioviana Baill. **Floresta**, [*S.l.*], v. 47, n. 4, p. 469-478. Disponível em: https://doi.org/10.5380/rf.v47i4.53988. Acesso em: 7 nov. 2024.

FORZZA, R. C. Projeto coordenado pelo Jardim Botânico do Rio de Janeiro. **Flora do Brasil,** 2020. Disponível em: https://dspace.jbrj.gov.br/jspui/handle/doc/118. Acesso em: 04 out. 2022.

FROMARD, F.; PUIG, H.; MARTY, J.; BETEOULLE, L.; CADAMURO, L. *Structure, above-ground biomass and dynamics of mangrove ecosystems: new data from French Guiana.* ***Oecologia***, [*S.l.*], , v. 115, p. 39-53, 1998. Disponível em: https://doi.org/10.1007/s004420050. Acesso em: 4 out. 2022.

FUJIMOTO, K.; ONO, K.; TABUCHI, R., LIHPAI, S. *Findings from long-term monitoring studies of Micronesian mangrove forests with special reference to carbon sequestration and sea-level rise.* ***Ecological Research***, [*S.l.*], 2022. Disponível em: https://doi.org/10.1111/1440-1703.12346. Acesso em: 4 out. 2022.

FUNDACIÓN SOLAR. **Elementos técnicos para inventários de carbono em uso do solo**. Colaboração Andrew Roy Edwin Castellanos. Guatemala, 2000.

GAO, B. *A normalized difference water index for remote sensing of vegetation liquid water from space.* ***Remote Sensing of Environment***, [*S.l.*], v. 58, n. 3, p. 257-266, 1996. Disponível em: https://doi.org/10.1016/S0034-4257(96)00067-3. Acesso em: 4 out. 2022.

GHOSH, S. M., BEHERA, M. D. *Aboveground Biomass Estimates of Tropical Mangrove Forest Using Sentinel-1 SAR coherence data - The superiority of deep learning over a semi-empirical model****. Computers & Geosciences***, *[S.l.*], v. 150, 2021. Disponível em: https://doi.org/10.1016/j.cageo.2021.104737. Acesso em: 4 out. 2022.

GITELSON, A. A; KAUFMAN, Y. J.; MERZLYAK, M. N. *Use of a green channel in remote sensing of global vegetation from EOS-MODIS.* ***Remote Sensing of Environment,*** *[S.l.*], v. 58, p. 289-298, 1996. Disponível em: https://doi.org/10.1016/S0034-4257(96)00072-7. Acesso em: 4 out. 2022.

GUZZI, A. **Biodiversidade do Delta do Parnaíba:** litoral piauiense. EDUFPI, Parnaíba, 2012. 466p.

HICKEY, S. M.; CALLOW, N. J.; PHINN, S.; LOVELOVK, C. E.; DUARTE, C. M. Spatial complexities in aboveground carbon stocks of a semi-arid mangrove community: *a remote sensing height-biomass-carbon approach.* ***Estuarine, Coastal and Shelf Science***, [*S.l.*], v. 200,

p. 194-201, 2018. Disponível em: https://doi.org/10.1016/j.ecss.2017.11.004. Acesso em: 4 out. 2022.

HUETE, A.R.; LIU, H. Q.; BATCHILY, K.; LEEUWEN, W.V. *A comparison of vegetation indices over a global set of TM images for EOS-MODIS*. ***Remote Sensing of Environment***, [*S. l.*], v. 59, n. 3, p. 440-451, 1997. Disponível em: https://doi.org/10.1016/S0034-4257(96)00112-5. Acesso em: 4 out. 2022.

HUETE, A. R. *A soil adjusted vegetation index (SAVI)*. ***Remote sensing of Environment,*** [*S. l.*], v. 25, n. 3, p. 295-309, 1988. Disponível em: https://doi.org/10.1016/0034-4257(88)90106-X. Acesso em: 4 out. 2022.

INSTITUTO CHICO MENDES DE CONSERVAÇÃO DA BIODIVERSIDADE (ICMBIO). **Atlas dos manguezais do Brasil**, Brasília: ICMBIO, 2018. ISBN 978-85-61842-75-8

INSTITUTO CHICO MENDES DE CONSERVAÇÃO DA BIODIVERSIDADE (ICMBIO). **Plano de manejo da área de proteção ambiental Delta do Parnaíba**, Brasília: ICMBIO, 2020. Disponível em: https://www.gov.br/icmbio/pt-br. Acesso em: 4 out. 2022.

JACHOWSKI, N. R. A; QUAK, M. S. Y; FRIESS, D. A.; DUANGNAMON, D.; WEBB, E. L.; ZIEGLER, A. D. *Mangrove biomass estimation in Southwest Thailand using machine learning*. ***Applied Geography***, [*S.l.*], v. 45, 311-321, p. 2013. Disponível em: https://doi.org/10.1016/j.apgeog.2013.09.024. Acesso em: 4 out. 2022.

KAUFFMAN, J. B.; DONATO, D. C. *Protocols for the measurement, monitoring, and reporting of structure, biomass and carbon stocks in mangrove forests. CIFOR Working Paper 86*. ***Environmental Science***. Center for International Forest Research, Bogor, Indonesia, 2012.

KAUFFMAN, J. B.; BERNARDINO, A. F.; FERREITA, T. O.; GIOVANNONI, L. R.; GOMES, L. E. de; ROMERO, D. J.; JIMENEZ, L. C. Z; RUIZ, F. *Carbon stocks of mangroves and salt marshes of the Amazon region. Brazil*. ***Biol Lett***, [*S.l.*], v. 14, p. 1–4, 2018. Disponível em: https://doi.org/10.1098/rsbl.2018.0208. Acesso em: 4 out. 2022.

KUWAE, T.; WATANABE, A.; YOSHIHARA, S.; SUEHIRO, F. *Implementation of blue carbon offset crediting for seagrass meadows, macroalgal beds, and macroalgae farming in Japan*. ***Revista Marine Policy,*** [*S.l.*], v. 138, p. 1-11, 2022. Disponível em: https://doi.org/10.1016/j.marpol.2022.104996. Acesso em: 4 out. 2022.

KUHN, M. J. K. ***Applied Predictive Modeling***. New York Springer, 2013. ISBN: 978-1-4614-6848-6

LI, A.; DHAKAL, S.; GLEN, N. F.; SPAETE, L. P.; SHINNEMAN, P. D. S.; ARKLE, R. S.; MCLLROY, S. K. *et al*. Lidar *Aboveground vegetation biomass estimates in Shrublands: prediction, uncertainties and application to coarser scales*, ***Remote Sensing***, [*S.l.*], v. 9, p1-19, 2017. Disponível em: https://doi.org/10.3390/rs9090903. Acesso em: 4 out. 2022.

LIMA JÚNIOR, C. de; ACCIOLY, L. J. de; GIONGO, V.; LIMA, R. L. F de A.; SAMPAIO, E. V. de S.; MENEZES, R. S. C. *Estimation of ''caatinga'' woody biomass using allometric equations and vegetation index*. ***Forest Sciences***. [*S.l.*], v. 42, n. 102, p. 289–298, 2014. Disponível em: https://ainfo.cnptia.embrapa.br/digital/bitstream/item/114649/1/ScientiaForestalis.pdf. Acesso em: 27 maio 2022.

LI, Y.; LI, C.; LIU, Z. *Forest aboveground biomass estimation using Landsat 8 and Sentinel-1A data with machine learning algorithms.* ***Scientific Reports***, [*S.l.*], v. 10, p. 1-22, 2020. Disponível em: https://doi.org/10.1038/s41598-020-67024-3. Acesso em: 27 maio 2022.

LUO, M.; WANG, Y.; XIE, Y.; ZHOU, L.; QIÃO, J.; QIU, S.; SUN, Y. *et al*. *Combination of Feature Selection and CatBoost for Prediction: The First Application to the Estimation of Aboveground Biomass.* ***Forests,*** [*S.l.*], v. 216, p. 1-21, 2021. Disponível em: https://doi.org/10.3390/f12020216. Acesso em: 27 maio, 2022.

LU, D. B. M.; MORAN, E. *Satellite estimation of aboveground biomass and impacts of forest stand structure. Photogr Eng* ***Remote Sens,*** [*S.l.*], v. 71, p. 967–974, 2005. Disponível em: https://ainfo.cnptia.embrapa.br/digital/bitstream/item/106870/1/1801.pdf. Acesso em: 30 mar. 2023.

MEIER, M.; SOUZA, E. de; FRANCELINO, M. R.; FERNANDES FILHO, I. E.; SCHAEFER, C. E. G. R. *Digital Soil Mapping Using Machine Learning Algorithms in a Tropical Mountainous Area.* ***Rev Bras Cienc Solo***, [*S.l.*], v. 42, 2018. Disponível em: https://doi.org/10.1590/18069657rbcs20170421. Acesso em: 4 out. 2022.

NAESSENS W, M. T.; NOPENS, I. *Critical review of membrane bioreactor models. Part 1: Biokinetic and filtration models.* ***Bioresource Technology****,* [*S.l.*], v. 122, p. 95–106, 2012. Disponível em: https://doi.org/10.1016/j.biortech.2012.05.070. Acesso em: 4 out. 2022.

NASCIMENTO, M. G. P. **Ecologia sistemática e sequestro de carbono em áreas de manguezal do Delta do Parnaíba, Maranhão, Brasil.** 2021. Tese (Doutorado) – Universidade Federal do Piauí, Centro de Ciências da Natureza, Programa Regional de Pós-Graduação em Desenvolvimento e Meio Ambiente, Teresina, 2021.

PANDIT, S. T. S.; DUBY, T. *Estimating Above-Ground Biomass in Sub-Tropical Buffer Zone Community Forests, Nepal, Using Sentinel 2 Data.* ***Remote sensing***, [*S.l.*], v. 10, n. 4, 2018. Disponível em: https://doi.org/10.3390/rs1004060. Acesso em: 4 out. 2022.

PEARSON, R. L.; MILLER, L. D. *Remote mapping of standing crop biomass for estimation of the productivity of shortgrass prairie, Pawnee National Grasslands, Colorado. In:* ***Proceedings of the 8th International Symposium on Remote Sensing of the Environment***, [*S.l.*], Ann Arbor, MI, v. 2, p. 1355-1379, 1972.

PERRY, C. R.; LAUTENSCHLAGER, L.F. *Functional equivalence of spectral vegetation indices.* ***Remote Sensing of Environnment***, [*S.l.*], v. 14, p. 169-182, 1984. Disponível em: https://doi.org/10.1016/0034-4257(84)90013-0. Acesso em: 4 out. 2022.

PHAM, T. D.; YOSHINO, K.; LE, N. N.; BUI, D. T. *Estimating aboveground biomass of a mangrove plantation on the Northern coast of Vietnam using machine learning techniques with an integration of ALOS-2 PALSAR-2 and Sentinel-2A data.* ***Remote Sens***, [*S.l.*], v. 39, n. 28, p. 7761-7788, 2018. Disponível em: https://doi.org/10.1080/01431161.2018.1471544. Acesso em: 4 out. 2022.

PINTO, L. M; VICENTE, A. F. C; VILLAÇA, I. M; BARAÇA, R.A. F; GOMES, R. L; MAGENTA, M. A. G; GIORDANO, F. *et al.* Sequestro de carbono atmosférico no bosque do manguezal da APA da Serra do Guararú, Guarujá-SP. UNISANTA **Bioscience**, [*S.l.*], v. 6 n. 1, p. 51-57, 2017. Disponível em: https://www.researchgate.net/publication/315225250. Acesso em: 4 out. 2022.

PORTELA, M. G. T.; ESPINDOLA, G. M. de; VALLADARES, G. S.; AMORIM, J. V. A.; FROTA, J. C. O. *Vegetation biomass and carbon stocks in the Parnaíba River Delta, NE Brazil*. ***Wetlands Ecology and Management***, *[S.l.*], v. 1, 2020. Disponível em: https://doi.org/10.1007/s11273-020-09735-y. Acesso em: 4 out. 2022.

PROJETO MAPBIOMAS. Coleção 4.0 da Série Anual de Mapas de Cobertura e Uso de Solo do Brasil. **Mapbiomas,** 2021. Disponível em: https://brasil.mapbiomas.org/colecoes-mapbiomas/. Acesso em: 15 out. 2023.

R CORE TEAM R: ***A Language and Environment for Statistical Computing***. Vienna, Austria: R Foundation for Statistical Computing, 2020. Disponível em: https://www.R-project.org/. Acesso em: 15 out. 2023.

ROUSE, J. W.; HAAS, R. H.; SCHELL, J. A.; DEERING, D.W.; HARLAN, J. C. ***Monitoring the vernal advancement of retrogradation (greenwave effect) of natural vegetation.*** NASA/GSFC, Type III, Final Report, Greenbelt, MD, 1974.

SABINS, F. F. ***Remote sensing:*** *principles and interpolation*. 3nd ed. New York : W. H. Freeman and Company, 1997.

SANTOS, I. R.; BELTRÃO, N. E. S; TRINDADE, A. R. Carbono "azul" nos manguezais amazônicos: conservação e valoração econômica. **Revista Iberoamericana de Economía Ecológica**, [*S.l.*], v. 31, n. 1, p. 18-28 . 2019. Disponível em: https://redibec.org/ojs. Acesso em: 15 out. 2023.

SANTOS, J. J. G.; BRETÓN, R. M. C.; BRETÓN, J. G. C.; HERNÁNDEZ, D. L. D.; JUNCO, R. C. S.; CARRIÓ, E. C. G. *Estimation of the carbon pool in soil and above-ground biomass within mangrove forests in Southeast Mexico using allometric equations.* ***Journal of Forestry Research***, [*S.l.*], v. 25 , n.1, p. 129-134, 2014. Disponível em: https://doi.org/10.1007/s11676-014-0437-2. Acesso em: 15 out. 2023.

SANTOS, H. G. dos. **Comparação da performance de algoritmos de machine learning para a análise preditiva em saúde pública e medicina**. 2018. Tese (Doutorado) – Universidade de São Paulo, São Paulo, 2018. Disponível em: https://doi.org/10.11606/T.6.2018.tde-09102018-132826. Acesso em: 7 nov. 2024.

SANTOS, H. V. S.; HOLLANDA, F. S. R.; SANTOS, T. de O.; ANDRADE, K. V. S. de; SANTA, M. B. S.; ESTRADA, G. C. D.; SOARES, M. L. G. *Allometric models for estimating the aboveground biomass of the mangrove Rhizophora mangle.* ***Brasilian Journal of Oceanography***, [*S.l.*], v. 65, n. 1, p. 44-53, 2017. Disponível em: https://doi.org/10.1590/S1679-87592017127006501. Acesso em: 15 out. 2023.

SELVARAJ, J. J.; PÉREZ, B. E. G. *Estimating mangrove aboveground biomass in the Colombian Pacific coast: A multisensor and machine learning approach.* ***Heliyon***, [*S.l.*], v. 9, 2023. Disponível em: https://doi.org/10.1016/j.heliyon.2023.e20745. Acesso em: 15 out. 2023.

SIQUEIRA, R. G.; VELOSO, G. V.; FERNANDES FILHO, E. I.; FRANCELINO, M. R. *Evaluation of machine learning algorithms to classify and map landforms in Antarctica Earth Surf.* ***Process. Landforms,*** [*S.l.*], v. 47, p. 367-382, 2021. Disponível em: https://doi.org/10.1002/esp.5253. Acesso em: 15 out. 2023.

SILVA, E. R. da. **Caracterização da área de proteção ambiental do delta do rio Parnaíba através de geotecnologias.** 2020. Trabalho de Conclusão de Curso (Graduação) – Universidade Federal do Ceará, Centro de Ciências Agrárias, Curso de Economia Ecológica, Fortaleza, 2020.

SILVA, E. J. da; ROSA, D. M.; VENDRUSCOLO, J.; CAVALHEIRO, W. C. S. Potencial de imagens do Sentinel-2 na estimativa da biomassa de Tectona grandis L.f. a Amazônia Ocidental Research, ***Society and Development***, [*S.l.*], v. 10, n. 11, p. 1-19, 2021. Disponível em: http://dx.doi.org/10.33448/rsd-v10i11.19491. Acesso em 18 de fev. de 2023.

TANG, W.; JIA, M.; SHI, J.; FRENG, W.; ZUO, H.; TRETTIN, C. *The assessment of mangrove biomass and carbon in west Africa: A spatially explicit analytical framework.* ***Wetlands Ecology Manage***, [*S.l.*], v. 24, p. 153-171, 2016. Disponível em: https://doi.org/10.1007/s11273-015-9474-7. Acesso em: 15 out. 2023.

TIAN, L.; TONG, Y.; CHENG, Y.; LI, M. *Drought diminishes aboveground biomass accumulation rate during secondary succession in a tropical forest on Hainan Island, China.* ***Forest Ecology and Management,*** [*S.l.*], v. 544, p. 121-221, 2023. Disponível em: https://doi.org/10.1016/j.foreco.2023.121222. Acesso em: 15 out. 2023.

TIAN, Y.; HUANG, H.; ZHOU, G.; ZHANG, Q.; TAO, J.; ZHANG, Y. *Aboveground Mangrove Biomass Estimation in Beibu Gulf Using Machine Learning and UAV* ***Remote Sensing***. ***The Science of the total environment***, [*S.l.*], v. 781, 2021. Disponível em: https://doi.org/10.1016/j.scitotenv.2021.146816. Acesso em: 15 out. 2023.

WANG, L.; ZHOU, X.; ZHU, X.; DONG, Z.; GUO, W. *Estimation of biomass in wheat using random forest regression algorithm and remote sensing data.* ***The Crop Journal***, [*S.l.*], v. v. 4, p. 212-219, 2016. Disponível em: https://doi.org/10.1016/j.cj.2016.01.008. Acesso em: 15 out. 2023.

WONG, C. J; JAMES, D.; BESAR, N. A; KAMLUN, K. U; TANGAH, J.; TSUYUKI, S.; PHUA, M. *Estimating Mangrove Above-Ground Biomass Loss Due to Deforestation in Malaysian Northern Borneo between 2000 and 2015 Using SRTM and Landsat Images.* ***Forests,*** [*S.l.*], v. 11, n. 9, 2020. Disponível em: https://doi.org/10.3390/f11091018. Acesso em: 15 out. 2023.

WU, C.; SHEN, H.; SHEN, A.; DENG, J. *Comparison of machinelearning methods for above-ground biomass estimation based on Landsat imagery.* ***Journal Appl Remote Sens***, [*S.l.*], v. 10, 2016. Disponível em: https://doi.org/10.1117/1.JRS.10.035010. Acesso em: 15 out. 2023.

XU, H. *Modification of normalised difference water index (NDWI) to enhance open water features in remotely sensed imagery.* ***International Journal of Remote Sensing,*** [*S.l.*], v. 27, n.14, p. 3025-3033, 2006. https://doi.org/10.1080/01431160600589179. Acesso em: 15 out. 2023.